Artificial intelligence solution to accelerate the acquisition of MRI images: impact on the therapeutic care in oncology in radiology and radiotherapy departments

Solution d'intelligence artificielle pour accélérer l'acquisition d'images IRM : impact sur la prise en charge thérapeutique en oncologie dans les services de radiologie et radiothérapie

Raphaëlle Lemaire[a], Charlotte Raboutet[b], Thomas Leleu[c], Cyril Jaudet[a], Loise Dessoude[c], Fernand Missohou[c], Yoann Poirier[b], Pierre-Yves Deslandes[d], Alexis Lechervy[e], Joëlle Lacroix[b], Ilyass Moummad[a,f], Stéphane Bardet[g], Juliette Thariat[c], Dinu Stefan[c] and Aurélien Corroyer-Dulmont[a,h]

[a] Medical Physics Department, Centre François Baclesse, 14000 Caen, France

[b] Radiology Department, Centre François Baclesse, 14000 Caen, France

[c] Radiotherapy Department, Centre François Baclesse, 14000 Caen, France

[d] Informatics Department, Centre François Baclesse, 14000 Caen, France

[e] UMR GREYC, Normandie Univ, UNICAEN, ENSICAEN, CNRS, 14000 Caen

[f] IMT Atlantique, Lab-STICC, UMR CNRS 6285, 29238 Brest, France

[g] Nuclear Medicine Department, Centre François Baclesse, 14000 Caen, France

[h] Université de Caen Normandie, CNRS, Normandie Université, ISTCT UMR6030, GIP CYCERON, 14000 Caen, France

Corresponding author:

Dr Aurélien Corroyer-Dulmont, Medical Physics Department, CLCC François Baclesse, 14000 Caen, France, phone: 33 2 31 45 50 50, fax: 33 2 31 47 02 22.

a.corroyer-dulmont@baclesse.unicancer.fr

Running title: Impact of a MRI AI solution on clinical radiology and radiotherapy processes

The author declare no conflict of interest

Running title: Impact of a MRI AI solution on clinical radiology and radiotherapy processes

Résumé

L'IRM est essentielle dans la prise en charge des tumeurs cérébrales. Cependant, les longs délais d'attente réduisent l'accessibilité des patients à cette modalité. La réduction du temps d'acquisition pourrait améliorer l'accès, mais au détriment de la résolution spatiale et de la qualité du diagnostic. Une solution d'intelligence artificielle (IA) disponible dans le commerce, SubtleMR®, peut augmenter la résolution des images acquises. L'objectif de cette étude prospective était d'évaluer l'impact de cet algorithme qui divise par deux le temps d'acquisition sur la détectabilité des lésions cérébrales en radiologie et radiothérapie.

Méthodes : Les IRM T1/T2 de 33 patients présentant des métastases cérébrales ou des méningiomes ont été analysées. Les images acquises rapidement possèdent une matrice divisée par deux qui divise par deux le temps d'acquisition. La qualité visuelle et la détectabilité des lésions des images IA ont été évaluées par des radiologues et des radiothérapeutes, ainsi que l'intensité des pixels et la taille des lésions.

Résultats : La qualité subjective de l'image est inférieure pour les images AI par rapport aux images de référence. Cependant, l'analyse de la détectabilité des lésions montre une spécificité de 1 et une sensibilité de 0,92 et 0,77 respectivement pour la radiologie et la radiothérapie. Les lésions non détectées sur l'image IA sont des lésions d'un diamètre inférieur à 4 mm et d'un contraste de rehaussement moyen en Gadolinium significativement plus faible.

Conclusions : Il est possible de diviser par deux les temps d'acquisition de l'IRM en utilisant l'algorithme commercial pour restituer les caractéristiques de l'image et obtenir une bonne spécificité et sensibilité pour les lésions de diamètre supérieur à 4 mm.

Mots clés : Intelligence Artificielle, Radiologie, Radiothérapie, Oncologie

Abstract

Purpose: MRI is essential in the management of brain tumours. However, long waiting times reduce patient accessibility. Reducing acquisition time could improve access but at the cost of spatial resolution and diagnostic quality. A commercially available artificial intelligence (AI) solution SubtleMR®, can increase the resolution of acquired images. The objective of this prospective study was to evaluate the impact of this algorithm which halve the acquisition time on the detectability of brain lesions in radiology and radiotherapy.

Methods: The T1/T2 MRI of 33 patients with brain metastases or meningiomas were analysed. Images acquired quickly have a matrix divided by two which halve the acquisition time. The visual quality and lesion detectability of the AI images were evaluated by radiologists and radiation oncologist as well as pixel intensity and lesions size.

Results: The subjective quality of the image is lower for the AI images compared to the reference images. However, the analysis of lesion detectability shows a specificity of 1 and a sensitivity of 0.92 and 0.77 for radiology and radiotherapy respectively. Undetected lesions on the IA image are lesions with a diameter less than 4mm and statistically low average Gadolinium enhancement contrast.

Conclusions: It is possible to half MRI acquisition times by using the commercial algorithm to restore the characteristics of the image and obtain good specificity and sensitivity for lesions with a diameter greater than 4 mm.

Keywords: Artificial intelligence, Radiology, Radiotherapy, Oncology

Introduction

Magnetic resonance imaging (MRI) is an important imaging modality tool in medicine for cancer diagnosis and treatment. Despite the presence of more than 800 MRI on French territory, the average time to obtain an appointment for this type of examination is about 32 days, higher than the waiting times desired by the 2014-2019 cancer plan of 20 days. Reducing acquisition time would increase MRI availability and reduce the time to obtain an appointment. There is therefore a real need to reduce this acquisition time to improve patient care. However, reducing acquisition time is feasible only with a reduction of the acquisition matrix or image averaging which decreases image quality [1]. Therefore, solutions to restore image quality after acquisition time reduction are needed.

Artificial intelligence (AI) and especially deep learning, a subdomain of AI, has seen an enormous advancements and application in medicine in recent years [2]. NYU Langone and Facebook AI Research collaborated on a research project called “fastMRI”, which consists of open datasets and benchmarks for accelerating MRI sequence acquisition. They focused on brain and knee [3–5], and recently on prostate data [6]. Other applications exist for these algorithms, ranging from image denoising to improving the rendering of exam images [7] to super-resolution [8]. A super-resolution algorithm has been validated by the Food and Drug Administration for routine clinical application, Subtle MR™. This solution has reduced scan time acquisition by 40 % in spinal MRI [9] and a 60 % in brain MRI in multicentre and multi-MRI studies [10]. To the best of our knowledge, only one study assessed the application of the AI solution in assessing brain lesions, using a cohort of 25 patients, a 45 % reduction in acquisition time was obtained with half of the number of phase-encode lines [11]. Despite

these findings, none have addressed how the associated decrease in resolution because of the shorter acquisition time, could potentially affect tumour delineation. In addition, no information is available on the lesion size threshold for detectability when using the AI solution. As it is a resampling problem for the algorithm, the issue could be to remove or to create some lesions, especially the smaller ones. For this reason, in this prospective study, we evaluated the impact of the AI solution, which halve the acquisition time on the therapeutic management of small lesions such brain metastases.

Materials and Methods

Patients

This prospective study was approved by the local institutional review board. Thirty-three patients presenting with brain metastases (BM) and meningioma (MG) referred to our oncological centre between August 2022 and March 2023 were included. No prior selection criteria was used, all patients referred to our centre, for diagnosis or treatment follow-up, during the period were enrolled. Post-Gadolinium (Gd) T1 and T2 FLAIR brain imaging were performed for initial diagnosis or treatment efficacy follow-up. MR-004, a national French institution (INDS) defining health research conduct guidelines was used for this study. All patients provided informed consent for the use of their data. The study population characteristics are shown in **Table 1**.

Magnetic Resonance Imaging (MRI) acquisition

MRI was performed on an AREA SIEMENS 1.5 Tesla magnet using a brain dedicated 16 channels coil with the patient in a supine position. Prior to the examination patients were

injected with 0.2 mL/kg of DOTAREM (500µmol/ml). After a shimming process and scout imaging scan, tumor gadolinium enhancement was detected with a post-Gd T1 brain sequence. T2 FLAIR sequences were also used to evaluate oedema. Each sequence was acquired in a clinical (reference, longer) and then in an accelerated way (half the time). Images obtained from the accelerated sequences were then processed with the commercial AI solution.

Clinical reference sequences: Post-Gd T1, (TR/TEeff=2070/3.15 msec; Angle=15°; NEX=1; 208 contiguous slices; resolution=0.5x0.5x1 mm; acquisition matrix = 512x512 pixels and acquisition time=4min48). T2 FLAIR, (TR/TEeff=9640/131 msec; Angle=150°; NEX=1; 24 contiguous slices; resolution=1.5x1.5x5 mm; acquisition matrix = 320x320 pixels and acquisition time=2min21).

Accelerated sequences: Post-Gd T1, (TR/TEeff=2070/3.15 msec; Angle=15°; NEX=1; 208 contiguous slices; resolution=0.5x0.5x1 mm; acquisition matrix = 256x256 pixels and acquisition time=2min39). T2 FLAIR, (TR/TEeff=9640/131 msec; Angle=150°; NEX=1; 24 contiguous slices; resolution=1.5x1.5x5 mm; acquisition matrix = 160x160 pixels and acquisition time=1min24).

Deep learning model

The commercially available deep learning model SubtleMR™, was used for resampling. SubtleMR™ is based on a U-Net deep convolutional neural network backbone that was previously trained on a large number of paired low- and high-resolution images acquired from a variety of vendors, field strengths, and institutions. A new series with the same nominal

resolution as the standard of care sequence was generated after applying the AI-enhanced algorithm. This model is used for inference, without any local fine-tuning or adaptation.

Image Analysis and processing

Visual analysis: Reference and AI reconstructed images were reviewed by one experienced radiologist and three experienced radiation oncologist on a Syngo.via viewing server (version VB 30A, Siemens Healthcare) and Raystation™ solution (V11.B) respectively. Readers attributed a global, whole-image quality (IQ) score to each MRI series: 1=poor; 2, 3=moderate; 4=good and 5=very good.

Semi-quantitative analysis:

Radiology: As part of routine image review, one radiologist evaluated the maximum length of each lesion using Syngo.via™. Comparison of this value was made between reference and AI reconstructed images.

Radiotherapy: Following a routine workflow in radiotherapy department, radiation oncologist delimited in 3D volume of interest (VOI) the volume of each lesion using Raystation™ solution (V11.B). Structural similarity index measure (SSIM) and Jaccard index were used to compare the VOI delimited by the radiation oncologist on reference and AI reconstructed images.

Global: One dimension imaging profiles from left to right part of the brain patients were made to compare accelerated and AI reconstruction impact. First order intensity evaluation was performed using mean, standard deviation, min, max, skewness, kurtosis, signal to noise ratio and absolute contrast. Specificity and sensitivity were evaluated to control potential radiologist and radiation oncologist failure to detect lesions after AI reconstruction. Finally, to evaluate the performance of the AI solution in comparison with the twice-shorter acquired

images, maps of change in pixel value between AI reconstructed and reference images were computed with ImageJ as follows:

$$\frac{abs(Postprocessing\ image - reference\ image)}{reference\ image} * 100$$

To compare difference in similarity between reference to accelerated and AI images, structural similarity index measure (SSIM) was used using the formula below:

$$SSIM(P_{\hat{Y}}, P_Y) = \frac{1}{N} \sum_{P_{\hat{Y}}\, P_Y} \frac{(2\mu_{P_{\hat{Y}}}\mu_{P_Y} + c_1)(2\sigma_{P_{\hat{Y}}}\sigma_{P_Y} + c_2)}{(\mu^2{}_{P_{\hat{Y}}} + \mu^2{}_{P_Y} + c_1)(\sigma^2{}_{P_{\hat{Y}}} + \sigma^2{}_{P_Y} + c_2)}$$

Where:

N : Number of batch over which SSIM has been averaged

μ_(P_Y) and μ_(P_Ŷ) : Mean of patches P_Y and P_Ŷ respectively

σ_(P_Y) and σ_(P_Ŷ) : Deviation of patches P_Y and P_Ŷ respectively

c_1 and c_2 : Constants

Statistical analyses

All data are expressed as mean±SD. Student's *t*-test was used to compare the different quantitative metrics between reference and AI reconstructed images. All the statistical analysis were performed using python [12] and SciPy library. All python codes used in the analysis is available on https://github.com/AurelienCD/Impact-of-AI-MRI-solution-on-clinical-routine.

Results

Visual analysis

The accelerated image with an acquisition matrix divided by two, present with low resolution as illustrated in **Figure 1**. AI reconstruction improves some details in the image with large

lesion (white arrow) easily distinguishable but smaller lesion (black arrow) suffering from loss of detail.

Radiologist image quality scores are presented in **Figure 2A**. Due to the loss of detail during the fast acquisition process not fully recover by the AI solution, radiologist IQ scores are lower for AI images compared to reference images (mean score 4.79 ± 0.43 vs 1.86 ± 0.77, ***p<0.001 for reference and AI images respectively). As presented in **Figure 2B**, radiation oncologist also evaluated the IQ of the reference and AI images. Results are similar but some AI image had the higher IQ score (mean score 3.94 ± 0.87 vs 2.72 ± 0.89, ***p<0.001 for reference and AI images respectively).

Further analysis of the differences between the three image groups, showed that right to left axial profile showed a better the ability of the AI solution to recover spatial variation initially lost by the accelerated acquisition (**Figure 3A**). As presented in **Figure 3B**, images obtained with accelerated acquisition resulted in few variations of signal intensity thoughtout the axial profile. Differences were observed between the signal differences in the centre region corresponding to the cerebral ventricles for the reference image and the accelerated image (light blue line vs dark blue line in **Figure 3B**). More interestingly, AI images reconstructed from the accelerated image acquisition was comparable to the reference image with similar amplitude variation, showing the ability of the AI solution to restore lost information (blue line vs light blue line in **Figure 3B**).

Semi-quantitative analysis

First order signal intensity analysis of the whole image was firstly performed and revealed a decrease in mean pixel value in accelerated and AI reconstructed images in comparison to

reference images (p<0.001, **Table 2**). No difference was found for minimal, maximal and skewness values whereas kurtosis decrease significantly (p<0.001). Interestingly, signal to noise ratio increased significantly in the AI image in comparison to reference image (p<0.05). To evaluate the ability of the AI solution to restore details lost by the accelerated images, difference maps between accelerated and reference and AI and reference were computed. **Figure 4** illustrates the pixel value difference between the reference, accelerated and AI images. The reference and accelerated image subtraction map notes a 60% difference in pixel values in the contrast enhanced area. Interestingly, the AI solution was able to restore the shape of the lesion with pixel value differences lower than 30 %. SSIM was then evaluated to compare the similarity of accelerated and AI images to the reference. As shown by **Figure 4**, SSIM was significantly higher in AI images in comparison to accelerated images (SSIM 0.5921 ± 0.0577 vs 0.5878 ± 0.0588, **p<0.01 for AI and accelerated images respectively).

Impact of the AI solution on the detectability of the lesions

In this section, we evaluated lesion detectability as part of the routine clinical assessment by radiologists and radiation oncologists. Radiologist evaluate the lesion max diameter while radiation oncologists volumetrically outline three- lesions for radiotherapy planning purposes.

Impact of AI solution on radiology department: As presented in **Figure 5**, lesion max diameters are similarly drawn by the radiologist in the reference and in the AI images. No statistical difference were observed in lesion max diameter (mean lesion max diameter (mm) 15.35 ± 16.60 vs 14.38 ± 14.62). However, two lesions were not detected by the radiologist in the AI images in comparison to the lesions detected using the reference lesion. This result leads to a specificity of 1 and a sensitivity of 0.92 in comparison to reference images. However, if we

analyse the lesions missed by the radiologist in the AI images, it appeared that these lesions are the smaller in dimension with max lengths of three and four millimetres respectively. These results highlight the presence of a threshold for minimum lesions size to be detected of 4 mm.

Impact of AI solution on radiotherapy department:

No significant differences were observed between volumes of interest drawn by the radiation oncologist on the reference and the AI images. However, five lesions were missed by the radiation oncologist in the AI images in comparison to the reference images. Specificity and sensitivity were respectively 1 and 0.77. As for the radiology part, lesions missed were smaller in dimension, with volumes below 0.12 cm^3. It can also be noted that these lesions have a significant lower contrast enhancement in comparison to the other lesions (absolute contrast 0.007 ± 0.0028 vs 0.0154 ± 0.0074 for AI and reference images respectively, $p<0.05$).

Discussion

Too long delays in acquiring MRI lead to a long waiting times for the patients in urgent need of medical interventions. Many research groups, MRI manufacturers or even start-ups are developing solutions to enable faster acquisition without losing the diagnostic quality of the images. In our study, we analysed one of these solutions, SubtleMR™. We specifically evaluated whether this solution is able to reconstruct an image acquired two times faster than the acquisition time in clinical routine without appreciable loss in image quality as required for the routine clinical management of these patients.

Image reconstruction time using SubtleMR™ was about 1 min 30 sec, which is 30 sec longer than previously reported in literature [9]. This difference could be explainable by the fact that the AI solution was performed on a remote computer, not directly on a GPU connected to the MRI. However, images transfer and processing did not required human intervention and therefore fits into a clinical workflow.

Concerning the visual analysis, Bash and colleagues [9], have shown similar image quality for reference and AI reconstructed images. In our study, radiologist and radiation oncologists found lower image quality for AI images. This difference with the literature may be due to the fact that the matrix is only divided by two on the phase encoding axis where we have chosen to divide it on the x and the y-axis to give a significant time acquisition reduction. However, as for the cited study, we show that the AI solution is able to restore image details, which were lost during the accelerated acquisition process.

Since the images used for testing in this study were acquired on a different MRI than that used to train SubtleMR™, an adaptation of the learned features to capture the characteristics of the different MRI could potentially improve results. The participants of the fastMRI 2020 challenge pointed out that fine-tuning is required before application to clinical data [5]. Sarasaen and colleagues [13] show that when transferring a model trained on a benchmark dataset, fine-tuning on a new MRI with one subject-specific prior planning scan, improves the reconstruction quality. Hu and colleagues show that fine-tuning reduces aliasing artefacts while also increasing PSNR, SSIM and decreasing NRMSE [14].

Concerning the semi-quantitative analysis, in literature studies [7,15] the values of signal intensity collected on the AI image are generally closer to the values in the reference image, than to that of the accelerated image. In our study, the phenomenon is also present. This observation was also valid for standard deviation, kurtosis and signal to noise ratio. Signal to

noise ratio increase because of a decrease in the noise in the AI reconstructed images as shown by other studies [16]. As for the study by Jin and colleagues [8], our results showed SSIM with reference images higher in AI images in comparison to accelerated images.

Concerning the impact of the AI solution on lesion detectability and delineation, max diameters and three-dimension delimitations by radiologist and radiation oncologist respectively were not significantly different using reference or AI images. This conclusion is in line with the literature showing that AI solutions need to be improved but are sufficient to safely use in clinical routine [2]. As we have shown in a previous study using an AI solution with PET imaging [17]), missed lesions correspond only to small lesions with low radiotracer uptake which will have limited impact on the clinical therapeutic care and patient outcome.

Finally, it is important to balance the performance of an AI solution applied on final MRI images in comparison to an AI algorithm developed using a raw MRI signal as K-space. In the literature, several articles use K-space images as input with better results, because more information can be found in that image rather than final MRI image [18–20]. However, in a clinical situation it is often not possible to have routine access to the k-space except for directly embedded AI solutions from the manufacturer.

Conclusion

In a busy MRI clinical department, the AI solution could be used to great effect to increase patient throughput without an appreciable decrease in resolution. This was demonstrated in the comparable assessment of brain lesions with diameters > 4 mm by oncologists and radiologists alike. Future multicentric studies, including other MRI sequences and tumour sites, are warranted.

Remerciement :

Cette étude a été financée par la Région Normandie. Les auteurs tiennent à remercier le Dr Nadia Falzone pour ses commentaires perspicaces et sa lecture technique du manuscrit. Ce travail n'a bénéficié d'aucune subvention spécifique émanant d'organismes commerciaux ou à but lucratif

References

[1] R. Obuchowicz, A. Piórkowski, A. Urbanik, M. Strzelecki, Influence of Acquisition Time on MR Image Quality Estimated with Nonparametric Measures Based on Texture Features., Biomed Res Int. 2019 (2019) 3706581. https://doi.org/10.1155/2019/3706581.

[2] P.M. Johnson, M.P. Recht, F. Knoll, Improving the Speed of MRI with Artificial Intelligence, Semin Musculoskelet Radiol. 24 (2020) 12–20. https://doi.org/10.1055/s-0039-3400265.

[3] J. Zbontar, F. Knoll, A. Sriram, T. Murrell, Z. Huang, M.J. Muckley, A. Defazio, R. Stern, P. Johnson, M. Bruno, M. Parente, K.J. Geras, J. Katsnelson, H. Chandarana, Z. Zhang, M. Drozdzal, A. Romero, M. Rabbat, P. Vincent, N. Yakubova, J. Pinkerton, D. Wang, E. Owens, C.L. Zitnick, M.P. Recht, D.K. Sodickson, Y.W. Lui, fastMRI: An Open Dataset and Benchmarks for Accelerated MRI, (2018) 1–35. http://arxiv.org/abs/1811.08839.

[4] F. Knoll, J. Zbontar, A. Sriram, M.J. Muckley, M. Bruno, A. Defazio, M. Parente, K.J. Geras, J. Katsnelson, H. Chandarana, Z. Zhang, M. Drozdzalv, A. Romero, M. Rabbat, P. Vincent, J. Pinkerton, D. Wang, N. Yakubova, E. Owens, C.L. Zitnick, M.P. Recht, D.K. Sodickson, Y.W. Lui, fastMRI: A Publicly Available Raw k-Space and DICOM Dataset of Knee Images for Accelerated MR Image Reconstruction Using Machine Learning, Radiol Artif Intell. 2 (2020) e190007. https://doi.org/10.1148/ryai.2020190007.

[5] M.J. Muckley, B. Riemenschneider, A. Radmanesh, S. Kim, G. Jeong, J. Ko, Y. Jun, H. Shin, D. Hwang, M. Mostapha, S. Arberet, D. Nickel, Z. Ramzi, P. Ciuciu, J.-L. Starck, J. Teuwen, D. Karkalousos, C. Zhang, A. Sriram, Z. Huang, N. Yakubova, Y.W. Lui, F. Knoll, Results of the 2020 fastMRI Challenge for Machine Learning MR Image Reconstruction., IEEE Trans Med Imaging. 40 (2021) 2306–2317. https://doi.org/10.1109/TMI.2021.3075856.

[6] R. Tibrewala, T. Dutt, A. Tong, L. Ginocchio, M.B. Keerthivasan, S.H. Baete, S. Chopra, Y.W. Lui, D.K. Sodickson, H. Chandarana, P.M. Johnson, FastMRI Prostate: A Publicly Available, Biparametric MRI Dataset to Advance Machine Learning for Prostate Cancer Imaging., ArXiv. (2023).

[7] I. Moummad, C. Jaudet, A. Lechervy, S. Valable, C. Raboutet, Z. Soilihi, J. Thariat, N. Falzone, J. Lacroix, A. Batalla, A. Corroyer-Dulmont, The Impact of Resampling and Denoising Deep Learning Algorithms on Radiomics in Brain Metastases MRI, Cancers (Basel). 14 (2021) 36. https://doi.org/10.3390/cancers14010036.

[8] Z. Jin, Q.-S. Xiang, Improving accelerated MRI by deep learning with sparsified complex data., Magn Reson Med. 89 (2023) 1825–1838. https://doi.org/10.1002/mrm.29556.

[9] S. Bash, B. Johnson, W. Gibbs, T. Zhang, A. Shankaranarayanan, L.N. Tanenbaum, Deep Learning Image Processing Enables 40% Faster Spinal MR Scans Which Match or Exceed Quality of Standard of Care : A Prospective Multicenter Multireader Study., Clin Neuroradiol. 32 (2022) 197–203. https://doi.org/10.1007/s00062-021-01121-2.

[10] S. Bash, L. Wang, C. Airriess, G. Zaharchuk, E. Gong, A. Shankaranarayanan, L.N. Tanenbaum, Deep Learning Enables 60% Accelerated Volumetric Brain MRI While Preserving Quantitative Performance:

A Prospective, Multicenter, Multireader Trial., AJNR Am J Neuroradiol. 42 (2021) 2130–2137. https://doi.org/10.3174/ajnr.A7358.

[11] J.D. Rudie, T. Gleason, M.J. Barkovich, D.M. Wilson, A. Shankaranarayanan, T. Zhang, L. Wang, E. Gong, G. Zaharchuk, J.E. Villanueva-Meyer, Clinical Assessment of Deep Learning-based Super-Resolution for 3D Volumetric Brain MRI., Radiol Artif Intell. 4 (2022) e210059. https://doi.org/10.1148/ryai.210059.

[12] Anaconda Software Distribution, (2020). https://docs.anaconda.com.

[13] C. Sarasaen, S. Chatterjee, M. Breitkopf, G. Rose, A. Nürnberger, O. Speck, Fine-tuning deep learning model parameters for improved super-resolution of dynamic MRI with prior-knowledge., Artif Intell Med. 121 (2021) 102196. https://doi.org/10.1016/j.artmed.2021.102196.

[14] Y. Hu, Y. Xu, Q. Tian, F. Chen, X. Shi, C.J. Moran, B.L. Daniel, B.A. Hargreaves, RUN-UP: Accelerated multishot diffusion-weighted MRI reconstruction using an unrolled network with U-Net as priors., Magn Reson Med. 85 (2021) 709–720. https://doi.org/10.1002/mrm.28446.

[15] C. Zhao, M. Shao, A. Carass, H. Li, B.E. Dewey, L.M. Ellingsen, J. Woo, M.A. Guttman, A.M. Blitz, M. Stone, P.A. Calabresi, H. Halperin, J.L. Prince, Applications of a deep learning method for anti-aliasing and super-resolution in MRI., Magn Reson Imaging. 64 (2019) 132–141. https://doi.org/10.1016/j.mri.2019.05.038.

[16] N. Kashiwagi, H. Tanaka, Y. Yamashita, H. Takahashi, Y. Kassai, M. Fujiwara, N. Tomiyama, Applicability of deep learning-based reconstruction trained by brain and knee 3T MRI to lumbar 1.5T MRI., Acta Radiol Open. 10 (2021) 20584601211023940. https://doi.org/10.1177/20584601211023939.

[17] K. Weyts, C. Lasnon, R. Ciappuccini, J. Lequesne, A. Corroyer-Dulmont, E. Quak, B. Clarisse, L. Roussel, S. Bardet, C. Jaudet, Artificial intelligence-based PET denoising could allow a two-fold reduction in [18F]FDG PET acquisition time in digital PET/CT., Eur J Nucl Med Mol Imaging. 49 (2022) 3750–3760. https://doi.org/10.1007/s00259-022-05800-1.

[18] D.J. Lin, P.M. Johnson, F. Knoll, Y.W. Lui, Artificial Intelligence for MR Image Reconstruction: An Overview for Clinicians., J Magn Reson Imaging. 53 (2021) 1015–1028. https://doi.org/10.1002/jmri.27078.

[19] M.P. Recht, J. Zbontar, D.K. Sodickson, F. Knoll, N. Yakubova, A. Sriram, T. Murrell, A. Defazio, M. Rabbat, L. Rybak, M. Kline, G. Ciavarra, E.F. Alaia, M. Samim, W.R. Walter, D.J. Lin, Y.W. Lui, M. Muckley, Z. Huang, P. Johnson, R. Stern, C.L. Zitnick, Using Deep Learning to Accelerate Knee MRI at 3 T: Results of an Interchangeability Study., AJR Am J Roentgenol. 215 (2020) 1421–1429. https://doi.org/10.2214/AJR.20.23313.

[20] B. Clifford, J. Conklin, S.Y. Huang, T. Feiweier, Z. Hosseini, A.L.M. Goncalves Filho, A. Tabari, S. Demir, W.-C. Lo, M.G.F. Longo, M. Lev, P. Schaefer, O. Rapalino, K. Setsompop, B. Bilgic, S. Cauley, An artificial intelligence-accelerated 2-minute multi-shot echo planar imaging protocol for comprehensive high-quality clinical brain imaging., Magn Reson Med. 87 (2022) 2453–2463. https://doi.org/10.1002/mrm.29117.

Table 1: Description of the patient cohort / Description de la cohorte de patient

Included patients (N)	33	Number
Sex	55%	Female %
Age (Y)	66.33 ± 12.35	Mean±SD
	[28-93]	[range]
Lesion origin		Number (%)
Brain metastases (BM) - *From Lung cancer* - *From Breast cancer* - *From Kidney cancer* - *From Digestive cancer* - *From Melanoma cancer* - *From Gynecologic cancer* - *From Pancreatic cancer*	28 (85%) - 12 (43%) - 5 (18%) - 2 (7%) - 1 (4%) - 4 (14%) - 3 (11%) - 1 (4%)	
Meningiomas	5 (15%)	
Total number of BM	94	Number
Number of BM per patient	1.5 ± 0.71	

Table 2: Semi-quantitative analysis of the signal intensity in the global image / Analyse semi-quantitative de l'intensité du signal dans l'image entière

	Mean (SD)	Min	Max	Skewness	Kurtosis	Signal to noise ratio

Reference image	189 (61.40)	203.6	626.5	-0.45	2.27	0.46
Accelerated image	165.73 (58.75) ***	178.5	514.7	-0.46	0.29 ***	0.71 *
AI image	166.91 (56.15) ***	179.2	506.6	-0.49	0.29 ***	0.70 *

Figure 1: Representative MRI of reference image, accelerated image and AI reconstructed image in brain presenting brain metastases. Large lesion (white arrow) and small lesion (black arrow) were distinguishable after the AI reconstruction process / Images représentatives d'une IRM cérébrale T1 post-Gd acquise dans le protocole de référence, rapidement et avec la reconstruction par IA. Les grandes lésions (flèche blanche) et les petites lésions (flèche noire) pouvaient être distinguées après le processus de reconstruction par IA.

Figure 2: Impact of AI reconstruction on visual MRI IQ. IQ score frequencies for reference MRI and AI reconstructed MRI based on radiologist (A) and radiation therapist (B) notations. 1=poor; 2, 3=moderate; 4=good and 5=very good. / Impact de la reconstruction par IA sur la qualité d'image notée par les radiologues (A) et par les radiothérapeutes (B). 1=médiocre ; 2, 3=modéré ; 4=bon et 5=très bien.

Figure 3: Axial profile signal intensity (A) for representative reference, accelerated and AI reconstructed images (B). / Profil axial (A) d'intensité d'images de référence, accélérée et reconstruite par IA (B)

Figure 4: Effect of accelerated acquisition and AI solution on BM signal intensity. Representative MRI of reference images (left), difference map with accelerated acquisition images (middle) and AI reconstruction images (right). / Impact de l'acquisition accélérée et de la solution AI sur l'intensité du signal des MC. IRM représentative des images de référence (à gauche), carte de différence entre les images d'acquisition accélérée et la référence (au milieu) et entre les images de reconstruction AI et la référence (à droite).

Figure 5: Impact of AI solution on lesion max diameters delimitation by radiologist / Impact de l'algorithme d'IA sur le plus grand diamètre de la lésion traçé par le radiologue

Lettre d'accompagnement/cover letter

Aurélien CORROYER-DULMONT, PhD
Chercheur-Ingénieur imagerie médicale et IA
Responsable scientifique du service de physique médicale, Centre François Baclesse
ISTCT UMR6030-CNRS, UNICAEN
3 Av. du Général Harris, 14000 Caen, France
E-mail: a.corroyer-dulmont@baclesse.unicancer.fr

Prof. Dr. Jean-Jacques Mazeron, Editeur en chef
Cancer/Radiothérapie
Hôpital Universitaire Pitie Salpetrière Service de Oncologie Radiothérapie, Paris

Nous vous serions reconnaissants de bien vouloir envisager une publication dans Cancer/Radiothérapie pour le manuscrit joint intitulé : « *Solution d'intelligence artificielle pour accélérer l'acquisition d'images IRM : impact sur la prise en charge thérapeutique en oncologie dans les services de radiologie et radiothérapie* » par Raphaëlle Lemaire, Charlotte Raboutet, Thomas Leleu, Cyril Jaudet, Loise Dessoude, Ferdinand Missohou, Yoann Poirier, Pierre-Yves Deslandes, Alexis Lechervy, Joëlle Lacroix, Ilyass Moummad, Stéphane Bardet, Juliette Thariat, Dinu Stefan et Aurélien Corroyer-Dulmont.

Les algorithmes d'intelligence artificielle (IA) disponibles dans le commerce ou intégrés dans les nouvelles IRM tentent d'accélérer le temps d'acquisition pour contrer les listes d'attente trop importantes. Cependant, on en sait peu sur comment ces algorithmes affecte la gestion thérapeutique du cancer, en particulier dans les services de radiologie et de radiothérapie. Dans ce manuscrit, nous avons évalué une solution d'IA disponible dans le commerce en routine clinique (solution SubtleMR™). Pour ce faire, nous avons évalué l'impact de la solution sur l'approche diagnostique faite par le radiologue et l'impact sur la délimitation du volume cible faite par le radiothérapeute. Une analyse quantitative a également été réalisée pour évaluer l'impact sur le contraste entre la tumeur et les tissus sains et l'intensité du signal. Dans cette étude prospective, nous avons montré que la solution d'IA donnait des images acquises deux fois rapidement avec une qualité d'image moindre par rapport à la référence, cependant, la délimitation tumorale (longueur maximum et volume cible) par les radiologues et les radiothérapeutes ne sont pas significativement différentes et la spécificité et la sensibilité étaient élevées. Les quelques lésions manquées dans les images AI ne concernent que de petites lésions ayant un impact secondaire sur la prise en charge du patient (inférieures à 4mm avec un rehaussement du signal gadolinium significativement plus faible).

Nous sommes convaincus que ces résultats seront d'un intérêt important pour le lectorat de Cancer/Radiothérapie. Nous vous remercions pour votre temps et votre considération.

Je certifie que tous les co-auteurs ont vu et sont d'accord avec le contenu du manuscrit. Je certifie également qu'aucun article similaire n'a été simultanément soumis pour publication ailleurs.

Bien cordialement,

Caen, le 19 Octobre 2023 Dr. Aurélien Corroyer-Dulmont, Ph.D

Tableau/Table1

Table 1: Description of the patient cohort / Description de la cohorte de patient

Included patients (N)	33	Number
Sex	55%	Female %
Age (Y)	66.33 ± 12.35	Mean±SD
	[28-93]	[range]
Lesion origin		Number (%)
Brain metastases (BM) - *From Lung cancer* - *From Breast cancer* - *From Kidney cancer* - *From Digestive cancer* - *From Melanoma cancer* - *From Gynecologic cancer* - *From Pancreatic cancer*	28 (85%) - 12 (43%) - 5 (18%) - 2 (7%) - 1 (4%) - 4 (14%) - 3 (11%) - 1 (4%)	
Meningiomas	5 (15%)	
Total number of BM	94	Number
Number of BM per patient	1.5 ± 0.71	

Tableau/Table2

Table 2: Semi-quantitative analysis of the signal intensity in the global image / Analyse semi-quantitative de l'intensité du signal dans l'image entière

	Mean (SD)	Min	Max	Skewness	Kurtosis	Signal to noise ratio
Reference image	189 (61.40)	203.6	626.5	-0.45	2.27	0.46
Accelerated image	165.73 (58.75) ***	178.5	514.7	-0.46	0.29 ***	0.71 *
AI image	166.91 (56.15) ***	179.2	506.6	-0.49	0.29 ***	0.70 *

Figure1

Click here to access/download;Figure;Fig1.pdf

FIGURE 1

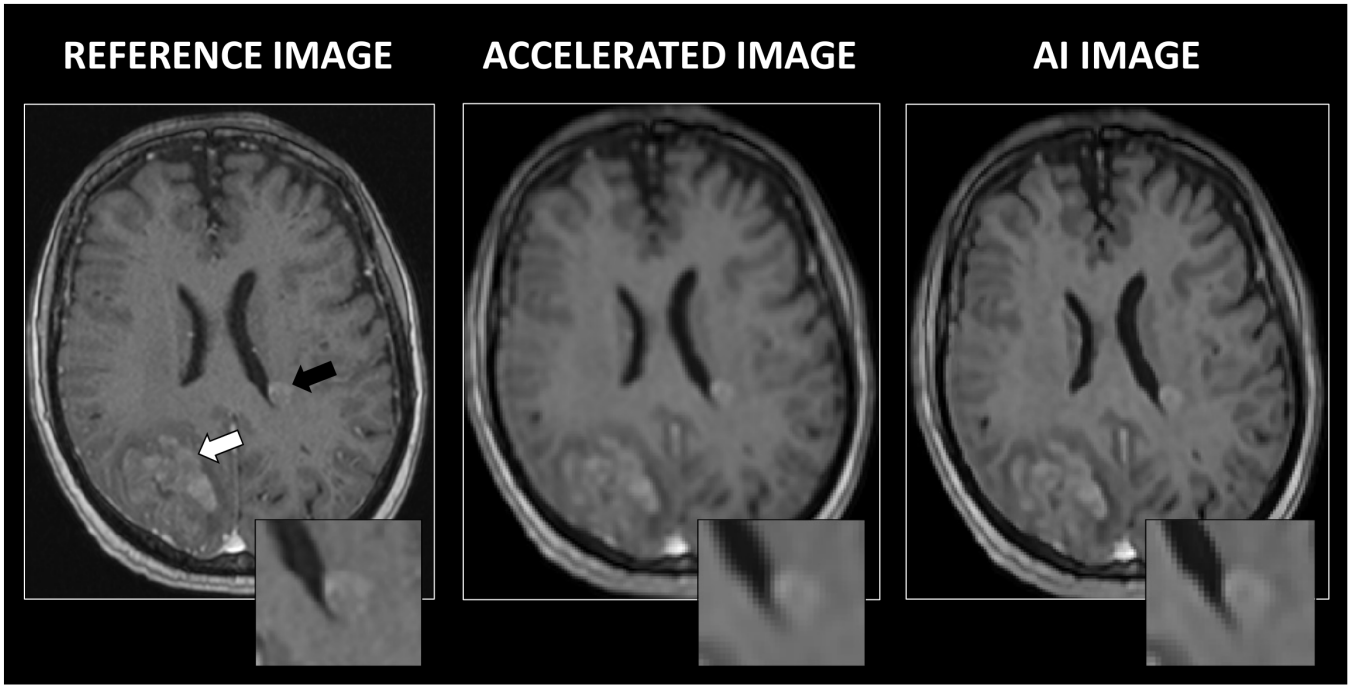

Figure2

Click here to access/download;Figure;Fig2.pdf

FIGURE 2

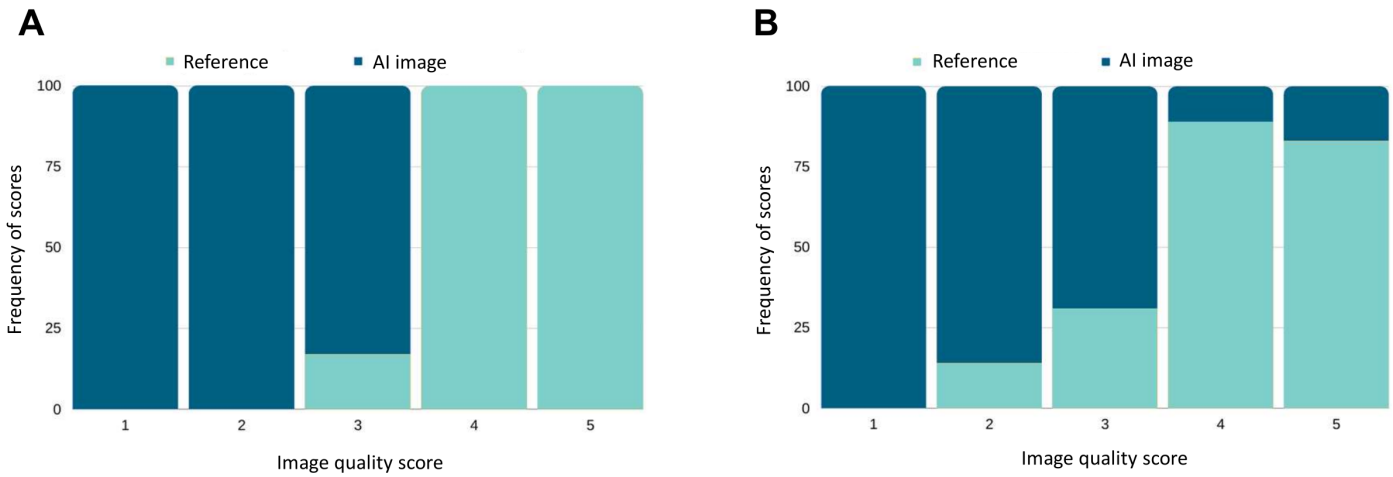

Figure3 Click here to access/download;Figure;Fig3.pdf

FIGURE 3

A

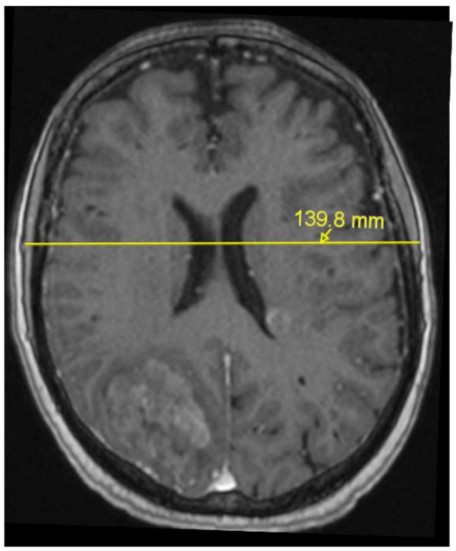

B

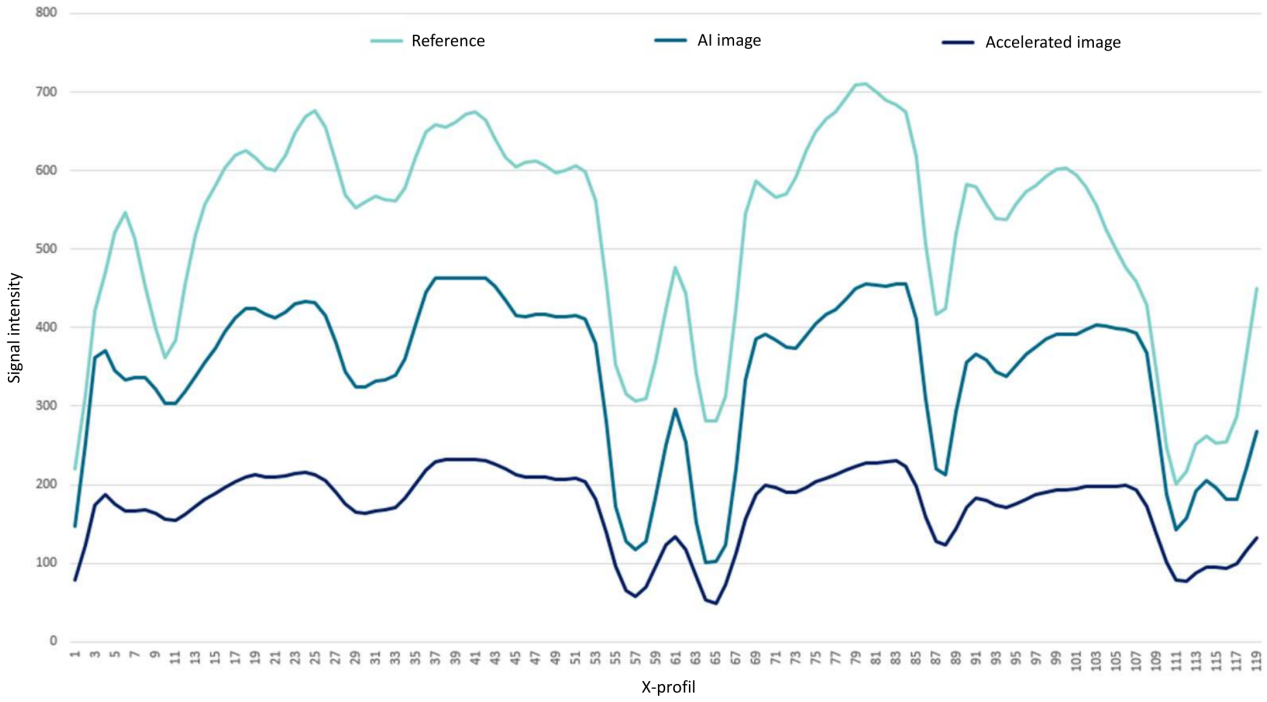

Figure4

Click here to access/download;Figure;Fig4.pdf

FIGURE 4

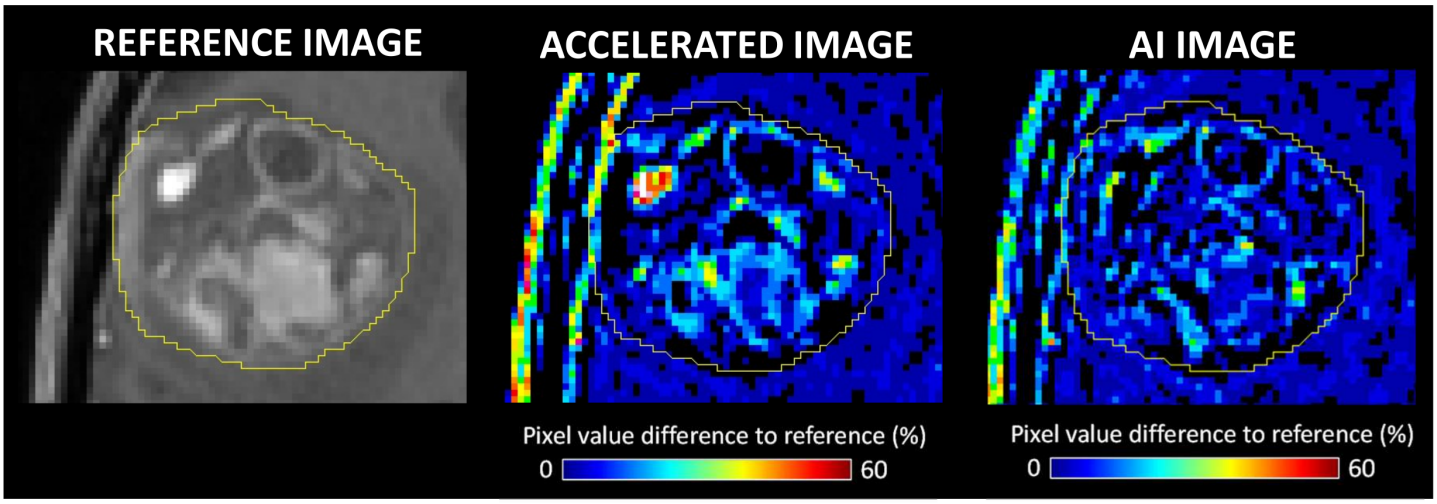

Figure5

Click here to access/download;Figure;Fig5.pdf

FIGURE 5

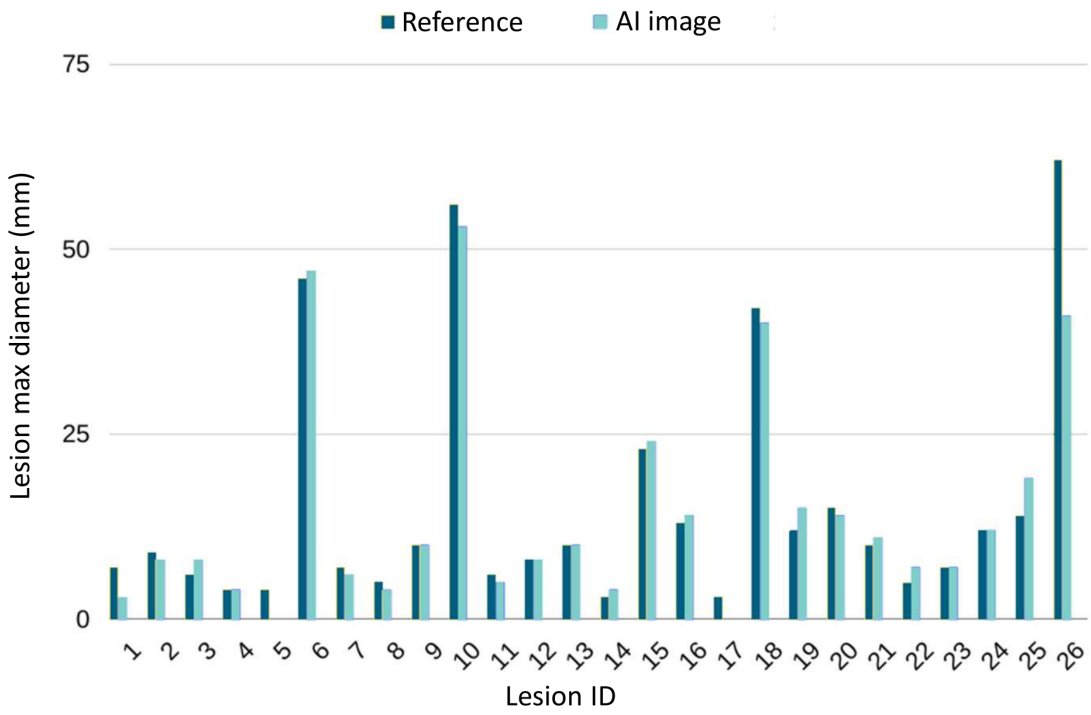

Legendes bilingues des tableaux et/ou figures/Translations of figure and/or table legends

Table 1: Description of the patient cohort / Description de la cohorte de patient

Table 2: Semi-quantitative analysis of the signal intensity in the global image / Analyse semi-quantitative de l'intensité du signal dans l'image entière

Figure 1: Representative MRI of reference image, accelerated image and AI reconstructed image in brain presenting brain metastases. Large lesion (white arrow) and small lesion (black arrow) were distinguishable after the AI reconstruction process / Images représentatives d'une IRM cérébrale T1 post-Gd acquise dans le protocole de référence, rapidement et avec la reconstruction par IA. Les grandes lésions (flèche blanche) et les petites lésions (flèche noire) pouvaient être distinguées après le processus de reconstruction par IA.

Figure 2: Impact of AI reconstruction on visual MRI IQ. IQ score frequencies for reference MRI and AI reconstructed MRI based on radiologist (A) and radiation therapist (B) notations. 1=poor; 2, 3=moderate; 4=good and 5=very good. / Impact de la reconstruction par IA sur la qualité d'image notée par les radiologues (A) et par les radiothérapeutes (B). 1=médiocre ; 2, 3=modéré ; 4=bon et 5=très bien.

Figure 3: Axial profile signal intensity (A) for representative reference, accelerated and AI reconstructed images (B). / Profil axial (A) d'intensité d'images de référence, accélérée et reconstruite par IA (B)

Figure 4: Effect of accelerated acquisition and AI solution on BM signal intensity. Representative MRI of reference images (left), difference map with accelerated acquisition images (middle) and AI reconstruction images (right). / Impact de l'acquisition accélérée et de la solution AI sur l'intensité du signal des MC. IRM représentative des images de référence (à gauche), carte de différence entre les images d'acquisition accélérée et la référence (au milieu) et entre les images de reconstruction AI et la référence (à droite).

Figure 5: Impact of AI solution on lesion max diameters delimitation by radiologist / Impact de l'algorithme d'IA sur le plus grand diamètre de la lésion traçé par le radiologue

Credit Author Statement

Les auteurs ne déclarent aucun conflit d'intérêt

Remerciement :

Cette étude a été financée par la Région Normandie. Les auteurs tiennent à remercier le Dr Nadia Falzone pour ses commentaires perspicaces et sa lecture technique du manuscrit. Ce travail n'a bénéficié d'aucune subvention spécifique émanant d'organismes commerciaux ou à but lucratif

References

[1] R. Obuchowicz, A. Piórkowski, A. Urbanik, M. Strzelecki, Influence of Acquisition Time on MR Image Quality Estimated with Nonparametric Measures Based on Texture Features., Biomed Res Int. 2019 (2019) 3706581. https://doi.org/10.1155/2019/3706581.

[2] P.M. Johnson, M.P. Recht, F. Knoll, Improving the Speed of MRI with Artificial Intelligence, Semin Musculoskelet Radiol. 24 (2020) 12–20. https://doi.org/10.1055/s-0039-3400265.

[3] J. Zbontar, F. Knoll, A. Sriram, T. Murrell, Z. Huang, M.J. Muckley, A. Defazio, R. Stern, P. Johnson, M. Bruno, M. Parente, K.J. Geras, J. Katsnelson, H. Chandarana, Z. Zhang, M. Drozdzal, A. Romero, M. Rabbat, P. Vincent, N. Yakubova, J. Pinkerton, D. Wang, E. Owens, C.L. Zitnick, M.P. Recht, D.K. Sodickson, Y.W. Lui, fastMRI: An Open Dataset and Benchmarks for Accelerated MRI, (2018) 1–35. http://arxiv.org/abs/1811.08839.

[4] F. Knoll, J. Zbontar, A. Sriram, M.J. Muckley, M. Bruno, A. Defazio, M. Parente, K.J. Geras, J. Katsnelson, H. Chandarana, Z. Zhang, M. Drozdzalv, A. Romero, M. Rabbat, P. Vincent, J. Pinkerton, D. Wang, N. Yakubova, E. Owens, C.L. Zitnick, M.P. Recht, D.K. Sodickson, Y.W. Lui, fastMRI: A Publicly Available Raw k-Space and DICOM Dataset of Knee Images for Accelerated MR Image Reconstruction Using Machine Learning, Radiol Artif Intell. 2 (2020) e190007. https://doi.org/10.1148/ryai.2020190007.

[5] M.J. Muckley, B. Riemenschneider, A. Radmanesh, S. Kim, G. Jeong, J. Ko, Y. Jun, H. Shin, D. Hwang, M. Mostapha, S. Arberet, D. Nickel, Z. Ramzi, P. Ciuciu, J.-L. Starck, J. Teuwen, D. Karkalousos, C. Zhang, A. Sriram, Z. Huang, N. Yakubova, Y.W. Lui, F. Knoll, Results of the 2020 fastMRI Challenge for Machine Learning MR Image Reconstruction., IEEE Trans Med Imaging. 40 (2021) 2306–2317. https://doi.org/10.1109/TMI.2021.3075856.

[6] R. Tibrewala, T. Dutt, A. Tong, L. Ginocchio, M.B. Keerthivasan, S.H. Baete, S. Chopra, Y.W. Lui, D.K. Sodickson, H. Chandarana, P.M. Johnson, FastMRI Prostate: A Publicly Available, Biparametric MRI Dataset to Advance Machine Learning for Prostate Cancer Imaging., ArXiv. (2023).

[7] I. Moummad, C. Jaudet, A. Lechervy, S. Valable, C. Raboutet, Z. Soilihi, J. Thariat, N. Falzone, J. Lacroix, A. Batalla, A. Corroyer-Dulmont, The Impact of Resampling and Denoising Deep Learning Algorithms on Radiomics in Brain Metastases MRI, Cancers (Basel). 14 (2021) 36. https://doi.org/10.3390/cancers14010036.

[8] Z. Jin, Q.-S. Xiang, Improving accelerated MRI by deep learning with sparsified complex data., Magn Reson Med. 89 (2023) 1825–1838. https://doi.org/10.1002/mrm.29556.

[9] S. Bash, B. Johnson, W. Gibbs, T. Zhang, A. Shankaranarayanan, L.N. Tanenbaum, Deep Learning Image Processing Enables 40% Faster Spinal MR Scans Which Match or Exceed Quality of Standard of Care : A Prospective Multicenter Multireader Study., Clin Neuroradiol. 32 (2022) 197–203. https://doi.org/10.1007/s00062-021-01121-2.

[10] S. Bash, L. Wang, C. Airriess, G. Zaharchuk, E. Gong, A. Shankaranarayanan, L.N. Tanenbaum, Deep Learning Enables 60% Accelerated Volumetric Brain MRI While Preserving Quantitative Performance:

A Prospective, Multicenter, Multireader Trial., AJNR Am J Neuroradiol. 42 (2021) 2130–2137. https://doi.org/10.3174/ajnr.A7358.

[11] J.D. Rudie, T. Gleason, M.J. Barkovich, D.M. Wilson, A. Shankaranarayanan, T. Zhang, L. Wang, E. Gong, G. Zaharchuk, J.E. Villanueva-Meyer, Clinical Assessment of Deep Learning-based Super-Resolution for 3D Volumetric Brain MRI., Radiol Artif Intell. 4 (2022) e210059. https://doi.org/10.1148/ryai.210059.

[12] Anaconda Software Distribution, (2020). https://docs.anaconda.com.

[13] C. Sarasaen, S. Chatterjee, M. Breitkopf, G. Rose, A. Nürnberger, O. Speck, Fine-tuning deep learning model parameters for improved super-resolution of dynamic MRI with prior-knowledge., Artif Intell Med. 121 (2021) 102196. https://doi.org/10.1016/j.artmed.2021.102196.

[14] Y. Hu, Y. Xu, Q. Tian, F. Chen, X. Shi, C.J. Moran, B.L. Daniel, B.A. Hargreaves, RUN-UP: Accelerated multishot diffusion-weighted MRI reconstruction using an unrolled network with U-Net as priors., Magn Reson Med. 85 (2021) 709–720. https://doi.org/10.1002/mrm.28446.

[15] C. Zhao, M. Shao, A. Carass, H. Li, B.E. Dewey, L.M. Ellingsen, J. Woo, M.A. Guttman, A.M. Blitz, M. Stone, P.A. Calabresi, H. Halperin, J.L. Prince, Applications of a deep learning method for anti-aliasing and super-resolution in MRI., Magn Reson Imaging. 64 (2019) 132–141. https://doi.org/10.1016/j.mri.2019.05.038.

[16] N. Kashiwagi, H. Tanaka, Y. Yamashita, H. Takahashi, Y. Kassai, M. Fujiwara, N. Tomiyama, Applicability of deep learning-based reconstruction trained by brain and knee 3T MRI to lumbar 1.5T MRI., Acta Radiol Open. 10 (2021) 20584601211023940. https://doi.org/10.1177/20584601211023939.

[17] K. Weyts, C. Lasnon, R. Ciappuccini, J. Lequesne, A. Corroyer-Dulmont, E. Quak, B. Clarisse, L. Roussel, S. Bardet, C. Jaudet, Artificial intelligence-based PET denoising could allow a two-fold reduction in [18F]FDG PET acquisition time in digital PET/CT., Eur J Nucl Med Mol Imaging. 49 (2022) 3750–3760. https://doi.org/10.1007/s00259-022-05800-1.

[18] D.J. Lin, P.M. Johnson, F. Knoll, Y.W. Lui, Artificial Intelligence for MR Image Reconstruction: An Overview for Clinicians., J Magn Reson Imaging. 53 (2021) 1015–1028. https://doi.org/10.1002/jmri.27078.

[19] M.P. Recht, J. Zbontar, D.K. Sodickson, F. Knoll, N. Yakubova, A. Sriram, T. Murrell, A. Defazio, M. Rabbat, L. Rybak, M. Kline, G. Ciavarra, E.F. Alaia, M. Samim, W.R. Walter, D.J. Lin, Y.W. Lui, M. Muckley, Z. Huang, P. Johnson, R. Stern, C.L. Zitnick, Using Deep Learning to Accelerate Knee MRI at 3 T: Results of an Interchangeability Study., AJR Am J Roentgenol. 215 (2020) 1421–1429. https://doi.org/10.2214/AJR.20.23313.

[20] B. Clifford, J. Conklin, S.Y. Huang, T. Feiweier, Z. Hosseini, A.L.M. Goncalves Filho, A. Tabari, S. Demir, W.-C. Lo, M.G.F. Longo, M. Lev, P. Schaefer, O. Rapalino, K. Setsompop, B. Bilgic, S. Cauley, An artificial intelligence-accelerated 2-minute multi-shot echo planar imaging protocol for comprehensive high-quality clinical brain imaging., Magn Reson Med. 87 (2022) 2453–2463. https://doi.org/10.1002/mrm.29117.

Table 1: Description of the patient cohort / Description de la cohorte de patient

Included patients (N)	33	Number
Sex	55%	Female %
Age (Y)	66.33 ± 12.35	Mean±SD
	[28-93]	[range]
Lesion origin		Number (%)
Brain metastases (BM) - *From Lung cancer* - *From Breast cancer* - *From Kidney cancer* - *From Digestive cancer* - *From Melanoma cancer* - *From Gynecologic cancer* - *From Pancreatic cancer*	28 (85%) - 12 (43%) - 5 (18%) - 2 (7%) - 1 (4%) - 4 (14%) - 3 (11%) - 1 (4%)	
Meningiomas	5 (15%)	
Total number of BM	94	Number
Number of BM per patient	1.5 ± 0.71	

Table 2: Semi-quantitative analysis of the signal intensity in the global image / Analyse semi-quantitative de l'intensité du signal dans l'image entière

	Mean (SD)	Min	Max	Skewness	Kurtosis	Signal to noise ratio

Reference image	189 (61.40)	203.6	626.5	-0.45	2.27	0.46
Accelerated image	165.73 (58.75) ***	178.5	514.7	-0.46	0.29 ***	0.71 *
AI image	166.91 (56.15) ***	179.2	506.6	-0.49	0.29 ***	0.70 *

Figure 1: Representative MRI of reference image, accelerated image and AI reconstructed image in brain presenting brain metastases. Large lesion (white arrow) and small lesion (black arrow) were distinguishable after the AI reconstruction process / Images représentatives d'une IRM cérébrale T1 post-Gd acquise dans le protocole de référence, rapidement et avec la reconstruction par IA. Les grandes lésions (flèche blanche) et les petites lésions (flèche noire) pouvaient être distinguées après le processus de reconstruction par IA.

Figure 2: Impact of AI reconstruction on visual MRI IQ. IQ score frequencies for reference MRI and AI reconstructed MRI based on radiologist (A) and radiation therapist (B) notations. 1=poor; 2, 3=moderate; 4=good and 5=very good. / Impact de la reconstruction par IA sur la qualité d'image notée par les radiologues (A) et par les radiothérapeutes (B). 1=médiocre ; 2, 3=modéré ; 4=bon et 5=très bien.

Figure 3: Axial profile signal intensity (A) for representative reference, accelerated and AI reconstructed images (B). / Profil axial (A) d'intensité d'images de référence, accélérée et reconstruite par IA (B)

Figure 4: Effect of accelerated acquisition and AI solution on BM signal intensity. Representative MRI of reference images (left), difference map with accelerated acquisition images (middle) and AI reconstruction images (right). / Impact de l'acquisition accélérée et de la solution AI sur l'intensité du signal des MC. IRM représentative des images de référence (à gauche), carte de différence entre les images d'acquisition accélérée et la référence (au milieu) et entre les images de reconstruction AI et la référence (à droite).

Figure 5: Impact of AI solution on lesion max diameters delimitation by radiologist / Impact de l'algorithme d'IA sur le plus grand diamètre de la lésion traçé par le radiologue